Noise in Charge Amplifiers—A g_m/I_D Approach

Enrique Alvarez, *Student Member, IEEE*, Diego Avila, *Student Member, IEEE*,
Hernan Campillo, *Student Member, IEEE*, Angelo Dragone, and Angel Abusleme, *Member, IEEE*

Abstract—**Charge amplifiers represent the standard solution to amplify signals from capacitive detectors in high energy physics experiments. In a typical front-end, the noise due to the charge amplifier, and particularly from its input transistor, limits the achievable resolution. The classic approach to attenuate noise effects in MOSFET charge amplifiers is to use the maximum power available, to use a minimum-length input device, and to establish the input transistor width in order to achieve the optimal capacitive matching at the input node. These conclusions, reached by analysis based on simple noise models, lead to sub-optimal results. In this work, a new approach on noise analysis for charge amplifiers based on an extension of the g_m/I_D methodology is presented. This method combines circuit equations and results from SPICE simulations, both valid for all operation regions and including all noise sources. The method, which allows to find the optimal operation point of the charge amplifier input device for maximum resolution, shows that the minimum device length is not necessarily the optimal, that flicker noise is responsible for the non-monotonic noise versus current function, and provides a deeper insight on the noise limits mechanism from an alternative and more design-oriented point of view.**

Index Terms—**Low-noise amplifiers, noise, nuclear physics instrumentation.**

I. INTRODUCTION

NOISE sets a fundamental limit on the resolution in measurements for particle physics experiments and radiation detectors. In a typical front-end circuit, consisting of a charge amplifier and a filter, the former is responsible for most of the noise present in the readout circuit signal path [1], [2]. Thus, a proper, integral design of the front-end for a particular detector ensures an adequate noise behavior [3]. Noise analysis for particle physics circuits is usually carried out by combining simple device noise models [4], [5] and the frequency response of the amplifier and the filter network [6]. The noise analysis outcome is the equivalent noise charge (ENC), measured in electrons, which represents the charge required at the detector to produce an output SNR of 1. Typically the input signal is a step of charge, or equivalently, a delta pulse of current with an area equal to the charge, and consequently the charge amplifier output voltage is

also a step. The filter, commonly referred to as pulse shaper, attenuates low and high frequencies, producing a time domain pulse. The signal is measured at the pulse peak, and noise is integrated over all frequencies to compute the ENC.

An interesting analysis methodology, presented in [7] and [8], is commonly used to simplify noise computation. The idea is to use the noise power spectral densities of the input device and detector (easy to compute due to the simplicity of noise equations) and tabulated results for the filter frequency behavior, conveniently pre-integrated and expressed as dimensionless numbers. This widely exploited technique allows a simple, insightful noise analysis, appropriate for design.

Typically, the low noise front-end design is achieved by following a simple recipe for the input transistor of the charge amplifier: maximum available current, optimal capacitance matching at the input node (which depends on the operation region) [9], and minimum-length input device [3], [10]. These guidelines, obtained from analysis on simple transistor noise models and neglecting flicker noise, produce acceptable but sub-optimal results, and fail to explain why minimum noise is not a monotonically decreasing function of the input transistor current.

Using more adequate models for current technologies and wider inversion coefficient range, in [2] the authors show that the guidelines previously stated do not necessarily produce optimal results, and conclude that flicker noise is responsible for the noise lowest limit. In [11], simplified EKV models were used to find several novel aspects of noise optimization for charge amplifiers. Both innovative ideas base their analysis on more realistic—and more complex—equations for the input transistor noise.

A new noise analysis technique, presented in this paper, is as follows: noise power spectral densities for a set of transistors are pre-computed by means of SPICE simulations, using the most comprehensive noise models available. The resulting curves are then properly scaled for the appropriate device parameters using the g_m/I_D technique [12], [13], conveniently modified in [14] to include noise. Finally, noise power spectral density can be obtained by using simple interpolations within the curves and the ENC can be integrated numerically. The main advantage of this approach is that it allows to work with simple and insightful analytical expressions, appropriate for design-oriented analysis.

This precise noise analysis technique can be used for the input-referred amplifier noise, either considering only the input device—in any operation region—or the noise contributions of more devices in the amplifier. Compared to previous methods, this one provides a better insight on the noise contributions by means of noise charts, adequate for a design process. The methodology was used to explore the design space of a charge

This article has been accepted for inclusion in a future issue of this journal. Content is final as presented, with the exception of pagination.

2

IEEE TRANSACTIONS ON NUCLEAR SCIENCE

TABLE I
NORMALIZED NOISE EQUATIONS

	I_n^2	$\hat{I}_n^2$
Thermal noise for strong inversion	$4k_B T \gamma g_m$	$4k_B T \gamma \left(\frac{g_m}{I_D} \right)$
Shot noise for weak inversion	$2qI_D$	$2q$
HSPICE $1/f$ noise (`NLEV=0`)	$\frac{K_F I_D^{A_F}}{C_{ox} L^2 f}$	$\frac{K_F I_D^{A_F - 1}}{C_{ox} L^2 f}$
HSPICE $1/f$ noise (`NLEV=2,3`)	$\frac{K_F g_m^2}{C_{ox} W L f^{A_F}}$	$\frac{K_F}{C_{ox} L f^{A_F}} \left(\frac{g_m}{I_D} \right)^2 \left(\frac{I_D}{W} \right)$
BSIM3 thermal noise	$\frac{4k_B T}{R_{DS} + L^2/(\mu|Q_{inv}|)}$	$\frac{4k_B T}{g_m R_{DS} + L^2 g_m/(\mu|Q_{inv}|)} \left(\frac{g_m}{I_D} \right)$
BSIM3 $1/f$ noise for strong inversion	$\frac{k_B T}{L^2 f^{E_F}} \left(\frac{q^2 \mu I_D W_A}{C_{ox}} + \frac{I_D^2 \Delta L_{clm} W_B}{qW} \right)$	$\frac{k_B T}{L^2 f^{E_F}} \left(\frac{q^2 \mu W_A}{C_{ox}} + \frac{\Delta L_{clm} W_B}{q} \left(\frac{I_D}{W} \right) \right)$

amplifier for particle physics experiments, allowing to reach and complement the conclusions from [2] regarding flicker noise contribution.

Without compromising the validity of the analysis only the preamplifier input device noise contribution will be considered, and generic BSIM3 noise models will be used. In real applications, secondary noise sources should be considered [15] as well as model parameters validated by measurements.

II. THE g_m/I_D METHODOLOGY AND NOISE ANALYSIS

Consider a transistor of width W, biased at a certain operation point with a drain current I_D, an overdrive voltage V_{OV}, transconductance g_m and gate-to-source capacitance C_{gs}. If another transistor with the same parameters and bias is connected in parallel, the compound transistor will have a drain current of $2 \cdot I_D$, an effective width of $2 \cdot W$, a gate-to-source capacitance of $2 \cdot C_{gs}$ and a transconductance of $2 \cdot g_m$, while V_{OV} and the level of inversion in the channel remain unchanged. The ratio g_m/I_D, which is a measure of the operation point of the transistor, also remains constant. Large values of g_m/I_D are related to subthreshold and weak inversion operation, whereas small values are related to strong inversion operation. Other ratios that can be mapped to the operation point are the transistor transit frequency ω_T (usually defined as g_m/C_{gs}) and the drain current density I_D/W. As shown in [14], MOSFET noise can also be mapped as a function of g_m/I_D by dividing the transistor drain current noise power spectral density I_n^2 by the drain current, or by multiplying the transistor gate voltage noise power spectral density V_n^2 by the drain current. Table I presents some examples of noise equations [5], [16], [17] and their normalized versions, where W_A and W_B are constants, and the other terms of each equation can be found in [16]. It can be shown that the term $g_m/|Q_{inv}|$ depends on g_m/I_D, therefore, it is clear that all normalized noise equations depend only on g_m/I_D.

It can be seen that the denominator of the BSIM3 equation for thermal noise has the term $g_m R_{DS}$, which is the transistor intrinsic gain, dependent on g_m/I_D and V_{DS}. The dependence on V_{DS} was added later in the BSIM model to make it more accurate, but at least as a first-order approximation the equation works for the normalization. However, if more accurate curves were necessary, several noise simulation can be done for different values of V_{DS}.
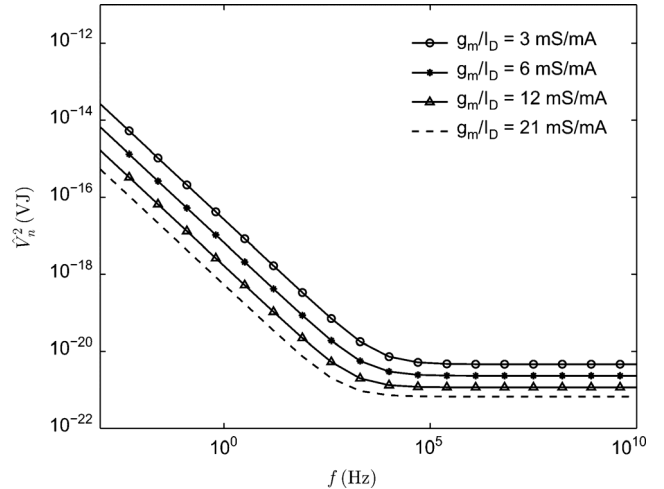

Fig. 1. $\hat{V}_n^2$ versus frequency for different values of g_m/I_D and $L = 0.18\,\mu\text{m}$. The curves were obtained using the BSIM3 MOSFET model.

Fig. 1 shows the transistor gate voltage noise power spectral density $\hat{V}_n^2$ for different values of g_m/I_D in a 0.18-μm technology. Low values of g_m/I_D imply large values of the corner frequency ω_c, which corresponds to the frequency at which the white and $1/f$ components of noise are equal. As pointed out in [14], when g_m/I_D decreases the I_D/W ratio increases and—for constant bias current—W decreases; as a consequence of a reduced gate area, flicker noise dominance extends to higher frequencies.

III. NOISE IN PULSE PROCESSOR FOR PARTICLE PHYSICS EXPERIMENTS

Fig. 2 shows a simplified, small-signal schematic of a typical front-end circuit for particle physics experiments. The detector is presented as a capacitance C_D, whereas the charge amplifier is shown as a voltage amplifier with open loop transfer function $A(j\omega)$, input capacitance C_{gs} and feedback capacitor C_F. Detector shot noise and amplifier voltage and current noise sources are included.

The ENC of the circuit in Fig. 2 can be computed as the square root of the ratio between the total output noise power and the output power produced by the charge of a single electron in a noiseless equivalent circuit. Since the detector shot noise depends only on the pulse shaper parameters, and here

This article has been accepted for inclusion in a future issue of this journal. Content is final as presented, with the exception of pagination.

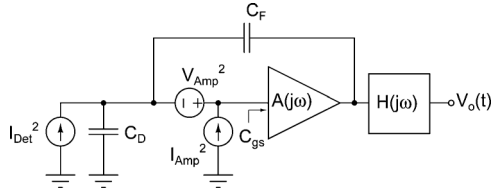ALVAREZ *et al.*: NOISE IN CHARGE AMPLIFIERS—A g_m/I_D APPROACH

3

Fig. 2. Schematic for noise analysis. Two noise sources are considered: detector shot noise and amplifier noise, represented as voltage and current noise; this includes both white and flicker noise.

it is assumed that these parameters have been already defined through other constraints (e.g., by the maximum allowed integration time), I_{Det}^2 will not be considered in the ENC^2 calculation.

Defining $C_K = C_D + C_F$, and $x = g_m/I_D$, the front-end output noise $V_{o,n}^2$, considering the amplifier noise (V_{Amp}^2 and $I_{Amp}^2 = \omega^2 C_{gs}^2 V_{Amp}^2$), can be expressed as

$$V_{o,n}^2 = \int_0^\infty \frac{(C_{gs}(x) + C_K)^2 \cdot |H(j\omega)|^2 \cdot V_{Amp}^2}{2\pi \cdot C_F^2} \, d\omega. \quad (1)$$

The computed ENC^2 is shown in (2), where q is the electron charge and $g(t)$ is the step response of $H(j\omega)$:

$$ENC^2 = \int_0^\infty \frac{(C_{gs}(x) + C_K)^2 \cdot |H(j\omega)|^2 \cdot V_{Amp}^2}{2\pi \cdot q^2 \cdot |\max[g(t)]|^2} \, d\omega. \quad (2)$$

Since the denominator of (2) is constant for given filter parameters, minimizing the ENC is equivalent to minimizing the numerator. Finally, the amplifier noise can be written as $V_{Amp}^2 = N(x,\omega)/I_D(x)$, where $N(x,\omega)$ corresponds to the total input-referred normalized noise power. Therefore, the objective function to minimize can be expressed as

$$F_o = \frac{(C_{gs}(x) + C_K)^2}{I_D(x)} \int_0^\infty |H(j\omega)|^2 \cdot N(x,\omega) \, d\omega. \quad (3)$$

The units of F_o are irrelevant for the purposes of this work, so they will be omitted.

IV. ENC MINIMIZATION

We will develop a brief example of ENC minimization for a charge amplifier design on a 0.18-μm technology. Let us consider a CR-RC filter, with a step response given by (4), where τ_p is the peaking time. The equation is normalized, so that the peak amplitude of its impulse response is 1:

$$g(t) = \frac{t}{\tau_p} e^{1-t/\tau_p}. \quad (4)$$

In order to compute ENC^2 as a function of I_D for different values of x and L, the magnitude of the filter transfer function must be computed first, and then introduced into (3). Fig. 3 shows F_o as a function of I_D for $L = 0.18 \, \mu$m, $K_F = 2 \cdot 10^{-29}$
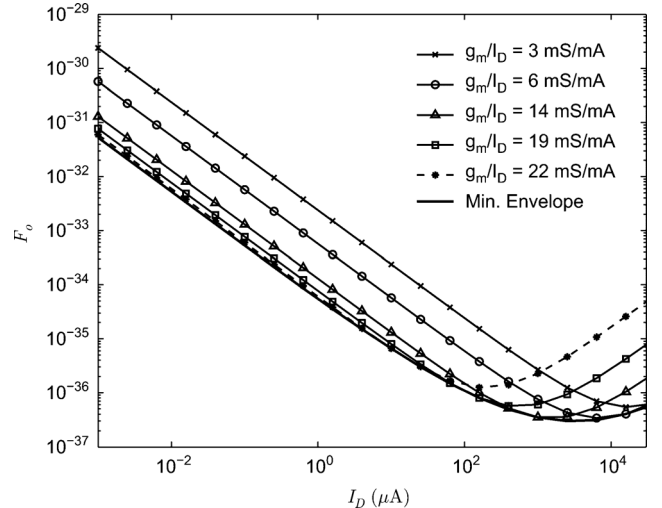

Fig. 3. F_o as a function of I_D for different operation points. The input device optimal operation point is at $x^* = 10.2$ mS/mA.

and a wide range of x.[1] Several conclusions can be drawn from this plot. For a constant x, L and filter parameters, the integral of (3) is constant, so minimizing F_o is equivalent to minimizing the function

$$F_{o2} = \frac{(C_{gs}(x) + C_K)^2}{I_D(x)}$$
$$= \frac{C_{gs}}{I_D}(x) \cdot C_{gs}(x) \left(1 + \frac{C_K}{C_{gs}(x)}\right)^2 \quad (5)$$

where C_{gs}/I_D is constant for a constant x. Hence, there is an optimal current for which total noise due to the amplifier is minimized. The optimal current value is that for which the condition $C_{gs} = C_K$ holds. On the other hand, for a constant current, the condition of capacitance matching at the front-end amplifier does not hold anymore for the point at which the total noise is minimized. Additionally, it can be observed that the minimum noise is not a monotonically-decreasing function of I_D, and this can be explained as follows: as shown in Fig. 3, low values of x produce v-shaped curves at the right of the plot, so as the current increases, each point of the minimum envelope corresponds to an operation point with a lower value of x than the previous point. As explained before, low values of x are related to high values of ω_c, thus, flicker noise becomes dominant when increasing the current and consequently the minimum envelope is not a monotonically-decreasing function of I_D. This fact can also be checked by extracting normalized power noise curves without considering flicker noise (i.e., setting $K_F = 0$ in the MOSFET SPICE models) and plotting the same curves as in Fig. 3. The results, presented in Fig. 4, show that, without the presence of flicker noise, the minimum envelope is a monotonically-decreasing function of I_D.

Further conclusions can be drawn by analyzing the minimum noise envelope for different channel lengths, as shown in Fig. 5. As it can be seen, using a minimum-length input device does

---

[1]Generic 0.18-μm transistor models available at MOSIS website [18] were used for this work. The value of K_F was selected so that the corner frequency is about 5 MHz.
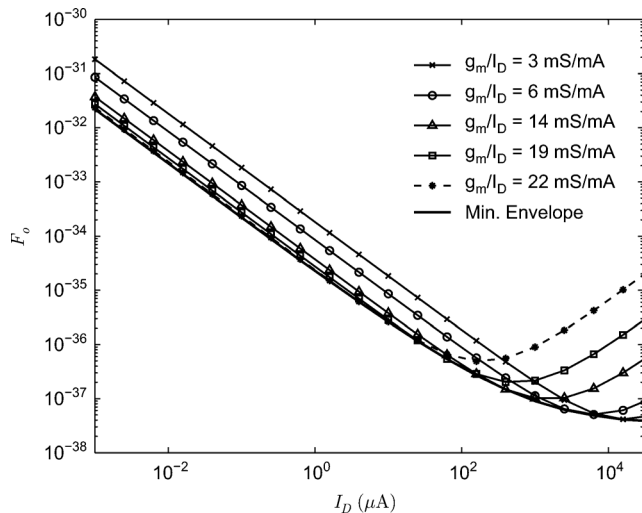
This article has been accepted for inclusion in a future issue of this journal. Content is final as presented, with the exception of pagination.

4   IEEE TRANSACTIONS ON NUCLEAR SCIENCE

Fig. 4. F_o as a function of I_D for different operation points and $K_F = 0$. The input device optimal operation point is at $x^* = 1.48\ \mathrm{mS/mA}$.
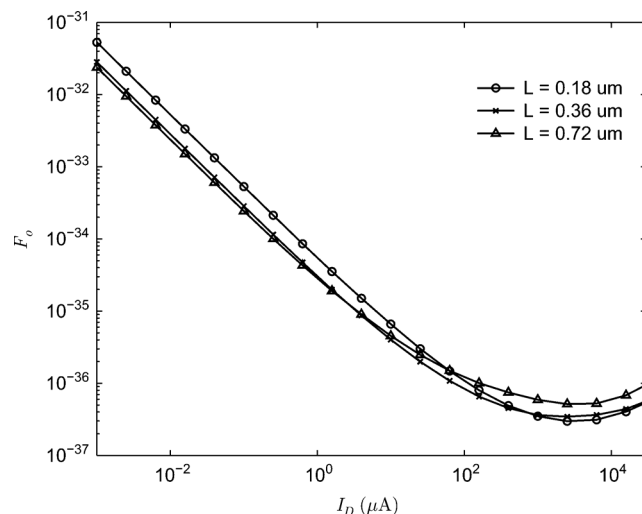

Fig. 5. Minimum envelope of F_o as a function of I_D for different length values.

not necessarily represent the optimal solution for every current or operation point.

V. COMPUTATION OF THE OPTIMAL g_m/I_D

As pointed out in the previous section, the 1:1 capacitive matching condition at the input of the front-end amplifier holds in the global optimum. Therefore, replacing $C_{gs} = C_K$ in (3) does not change the optimal solution of the minimization problem. Consequently, $I_D(x)$ can be expressed as

$$ I_D(x) = \frac{I_D}{C_{gs}}(x) \cdot C_K. \tag{6} $$

Using (6) in (3) and eliminating the constant terms, the minimization problem to solve becomes

$$ \mathrm{MIN}_x\ \frac{\int_0^\infty |H(j\omega)|^2 \cdot N(x,\omega)\,\mathrm{d}\omega}{\frac{I_D}{C_{gs}}(x)}. \tag{7} $$

By taking the derivative of (7) with respect to x and equating to zero, the condition for the optimal value of the input device
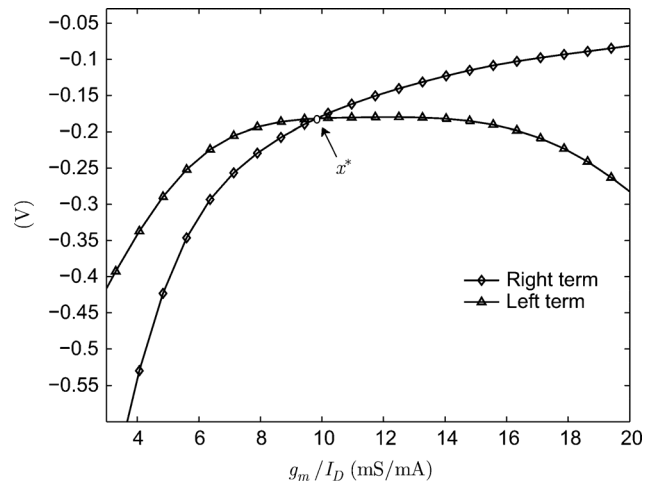

Fig. 6. Both terms of (8). The intersection point, which represents the input device optimal operation point, is at $x^* = 9.83\ \mathrm{mS/mA}$.

operation point x^*, for which the ENC^2 is minimum, can be determined:

$$ \frac{\frac{I_D}{C_{gs}}{}'(x^*)}{\frac{I_D}{C_{gs}}(x^*)} = \frac{\int_0^\infty |H(j\omega)|^2 \cdot N'(x^*,\omega)\,\mathrm{d}\omega}{\int_0^\infty |H(j\omega)|^2 \cdot N(x^*,\omega)\,\mathrm{d}\omega}. \tag{8} $$

In Fig. 6, left and right terms of (8) are shown for the same conditions of Fig. 3, where the intersection point of the curves, which represents the optimal value x^*, is pointed out. Although this condition allows to find x^* with an error of 3.6% compared to the solution found graphically in Fig. 3, it requires generating look-up tables for noise considering a particular filter transfer function, which is impractical for its use in a design-oriented methodology.

As shown in the Appendix, (8) can be simplified, for strong inversion operation, to

$$ \frac{\omega_T'(x^*)}{\omega_T(x^*)} = \frac{\omega_c'(x^*)}{\frac{a_w}{\tau_p a_f} + \omega_c(x^*)} \tag{9} $$

and for weak inversion operation to

$$ \frac{\omega_T'(x^*)}{\omega_T(x^*)} = -\frac{1}{x^*} + \frac{\omega_c'(x^*)}{\frac{a_w}{\tau_p a_f} + \omega_c(x^*)} \tag{10} $$

where $\omega_T(x)$ is the input device transit frequency, $\omega_c(x)$ is the input device corner frequency, a_w is the filter white noise coefficient and $a_f(A_F)$ is the filter flicker noise coefficient as a function of the flicker noise coefficient, A_F[2].

The conditions shown in (9) and (10) establish the lower (x_s^*, for strong inversion operation) and upper (x_w^*, for weak inversion operation) limits of x^*, respectively. Then x^* can be computed as the weighted average of x_s^* and x_w^*. The weight of each factor depends on how dominant the flicker noise is. High values of ω_c move the v-shaped curves to the left of the F_o versus I_D plot (see Fig. 3), reaching high values of x^*—weak inversion operation—meanwhile low values of ω_c move the v-shaped curves to the right of the F_o versus I_D plot, reaching low values of x^*—strong inversion operation.

In Fig. 7 both terms of (9) and (10) are shown for the same conditions of Fig. 3. The intersection points of the curves, which
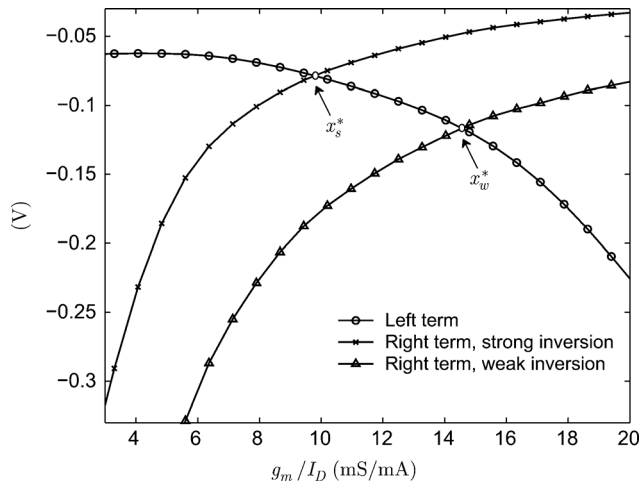
Fig. 7. Left term of (9) and (10), and both right terms. The intersection points, which represent the input device optimal operation point for each operation region, are $x_s^* = 9.78$ mS/mA and $x_w^* = 14.5$ mS/mA.

represent x_s^* and x_w^*, are pointed out. The optimal operation point, x^*, lays in between these boundaries. For simplicity in this specific case, considering that the value of x^* obtained from Fig. 3 suggests operation close to strong inversion, x_s^* could be used as an initial estimation with an additional advantage: filter and noise data are obtained independently, the first one from normalized filter tables and the second one from normalized noise power curves as functions of x. It is worth mentioning that the data must be carefully manipulated, since (8)–(10) are sensitive to numerical approximations.

Typical values of a_w/a_f are between 1.3 and 2.3 [2], thus the denominator of (9) can be simplified to $\approx 2/\tau_p + \omega_c(x^*)$ since τ_p is the responsible for the order of magnitude of the factor $a_w/\tau_p a_f$. In this particular case, the result obtained for x^* does not change significantly ($x^* = 9.98$ mS/mA for $a_w/a_f = 1.3$ and $x^* = 9.29$ mS/mA for $a_w/a_f = 2.3$). In case the noise specifications to meet are not too stringent, an additional simplification can be tolerated and an approximate surround of the optimal operation point of the front-end input device can be determined solely by using the pulse peaking time of the filter and ignoring the pulse shape. Additionally, it can be observed that flicker noise, which is responsible of the non monotonicity of the noise for high currents, is related to the pulse peaking time magnitude as follows: lower values of τ_p in (9) imply lower values of x^*, which are related to high values of ω_c. Therefore, when τ_p decreases, flicker noise contribution increases.

Finally, the conditions expressed in (9) and (10) reveal that the existence of a noise minimum is related to the sensitivity of ω_T with respect to x, and somehow to the sensitivity of ω_c with respect to x.

VI. CONCLUSION

This work shows a different view on a widely studied problem, noise optimization for particle physics electronics. The approach followed is based on an extension of the g_m/I_D methodology to allow noise analysis.

The results found show that, although capacitance matching represents the minimum noise for constant g_m/I_D, it is not a Pareto-optimal solution for low noise and low power circuits, where the power budget is limited; instead, lower capacitance and a different operation point is preferred. It is also shown that the device length optimization requires further study, because minimum length does not necessarily provide the optimal solution.

This work also presents an analysis on the dependence of the noise limit (assuming infinite power available) on flicker noise, and shows a method that allows to compute the operation point and current for which minimum noise is achieved, based only on technology data and filter parameters. This methodology provides a new insight on the impact of flicker noise in electronic systems for radiation detection. This work evidences that flicker noise is related with the existence of a finite current for which noise is minimum, and also outlines the relation between flicker noise and the filter peaking time.

APPENDIX
OPTIMAL CONDITION DERIVATION

Given that

$$\frac{I_D}{C_{gs}}(x) = \frac{1}{x} \cdot \frac{g_m}{C_{gs}}(x) \tag{11}$$

the left term of (8) can be expressed as

$$\frac{\frac{I_D}{C_{gs}}'(x)}{\frac{I_D}{C_{gs}}(x)} = \frac{\omega_T'(x)}{\omega_T(x)} - \frac{1}{x} \tag{12}$$

where $\omega_T(x)$ is the input device transit frequency (defined as g_m/C_{gs}). To simplify the right term of (8), a modified expression of $N(x, \omega)$ is necessary. Without loss of generality, the flicker noise component dependency on the frequency can be assumed to be $1/\omega^{A_F}$, where A_F is the flicker noise coefficient. Thus, $N(x, \omega)$ can be written as

$$N(x, \omega) = W(x) + F(x) \cdot \frac{1}{\omega^{A_F}} \tag{13}$$

where $W(x)$ is the white noise contribution and $F(x)/\omega^{A_F}$ is the $1/f$ noise contribution. Both $W(x)$ and $F(x)$ are constant for a given operation point, and they are related to each other through the corner frequency $\omega_c(x)$:

$$F(x) = \omega_c(x)^{A_F} W(x). \tag{14}$$

Considering the above simplifications, $N(x, \omega)$ can be finally expressed as

$$N(x, \omega) = W(x) \left(1 + \left(\frac{\omega_c(x)}{\omega} \right)^{A_F} \right) \tag{15}$$

and its derivative can be expressed as

$$N'(x, \omega) = W'(x) \left(1 + \left(\frac{\omega_c(x)}{\omega} \right)^{A_F} \right)$$
$$+ W(x) \frac{A_F \cdot \omega_c'(x) \cdot \omega_c(x)^{A_F - 1}}{\omega^{A_F}}. \tag{16}$$

Furthermore, the normalization $t = t'/\tau_p$ can be applied on the filter pulse response. This allows to work with tables of filter

This article has been accepted for inclusion in a future issue of this journal. Content is final as presented, with the exception of pagination.

6   IEEE TRANSACTIONS ON NUCLEAR SCIENCE

coefficients that depend only on the pulse shape, thus, the condition to find x^* can be expressed as

$$\frac{\omega'_T(x^*)}{\omega_T(x^*)} - \frac{1}{x^*} = \frac{W'(x^*)}{W(x^*)} + \frac{A_F \cdot \omega'_c(x^*) \cdot \omega_c(x^*)^{A_F - 1}}{\frac{a_w}{\tau_p^{A_F} a_f(A_F)} + \omega_c(x^*)^{A_F}} \quad (17)$$

where a_w is the white noise coefficient and $a_f(A_F)$ is the flicker noise coefficient [2]. These coefficients can be computed as

$$a_w = \frac{1}{2\pi \left| \max \left[g \left(\frac{t'}{\tau_p} \right) \right] \right|^2} \int_0^\infty |H(jy)|^2 \, \mathrm{d}y \quad (18)$$

$$a_f(A_F) = \frac{1}{2\pi \left| \max \left[g \left(\frac{t'}{\tau_p} \right) \right] \right|^2} \int_0^\infty \frac{|H(jy)|^2}{y^{A_F}} \, \mathrm{d}y \quad (19)$$

where $y = \tau_p \omega$.

Assuming $W(x) \propto x^{-1}$ (evident from the thermal noise models of Table I) and $A_F \approx 1$, for strong inversion operation, the expression in (17) can be further simplified to

$$\frac{\omega'_T(x^*)}{\omega_T(x^*)} = \frac{\omega'_c(x^*)}{\frac{a_w}{\tau_p a_f} + \omega_c(x^*)}. \quad (20)$$

Finally, assuming $W(x) \propto x^{-2}$ (see Table I) and $A_F \approx 1$, for weak inversion operation, the expression in (17) can be further simplified to

$$\frac{\omega'_T(x^*)}{\omega_T(x^*)} = -\frac{1}{x^*} + \frac{\omega'_c(x^*)}{\frac{a_w}{\tau_p a_f} + \omega_c(x^*)}. \quad (21)$$

REFERENCES

[1] G. De Geronimo, P. O'Connor, V. Radeka, and B. Yu, "Front-end electronics for imaging detectors," *Nucl. Instrum. Meth. Phys. Res.*, pp. 192–199, 2001.

[2] G. De Geronimo and P. O'Connor, "MOSFET optimization in deep submicron technology for charge amplifiers," *IEEE Trans. Nucl. Sci.*, vol. 52, no. 6, pp. 3223–3232, Dec. 2005.

[3] W. Sansen and Z. Chang, "Limits of low noise performance of detector readout front ends in CMOS technology," *IEEE Trans. Circuits Syst.*, vol. 37, no. 11, pp. 1375–1382, Nov. 1990.

[4] P. R. Gray, P. J. Hurst, S. H. Lewis, and R. G. Meyer, *Analysis and Design of Analog Integrated Circuits*, 4th ed.   New York: Wiley, 2001.

[5] B. Razavi, *Design of Analog CMOS Integrated Circuits*.   New York: McGraw-Hill, 2002.

[6] H. Spieler, *Semiconductor Detector Systems*.   Oxford, U.K.: Oxford Univ. Press, 2005.

[7] F. S. Goulding, "Pulse-shaping in low-noise nuclear amplifiers: A physical approach to noise analysis," *Nucl. Instrum. Meth.*, vol. 100, pp. 493–504, 1972.

[8] V. Radeka, "Low-noise tecniques in detectors," *Ann. Rev. Nucl. Part. Sci.*, vol. 38, pp. 217–277, 1988.

[9] P. O'Connor and G. De Geronimo, "Prospects for charge sensitive amplifiers in scaled cmos," in *IEEE Nuclear Science Symp. Conference Record 1999*, 1999, vol. 1, pp. 88–93.

[10] V. Radeka, "Semiconductor position-sensitive detectors," *Nucl. Instrum. Meth. Phys. Res. Section A: Accelerators, Spectrometers, Detectors and Associated Equipment*, vol. 226, no. 1, pp. 209–218, Sep. 1984.

[11] P. Grybos, M. Idzik, and A. Skoczen, "Design of low noise charge amplifier in sub-micron technology for fast shaping time," *Analog Integr. Circuits Signal Process.*, vol. 49, no. 2, pp. 107–114, 2006.

[12] F. Silveira, D. Flandre, and P. Jespers, "A g_m/I_D based methodology for the design of cmos analog circuits and its application to the synthesis of a silicon-on-insulator micropower OTA," *IEEE J. Solid-State Circuits*, vol. 31, no. 9, pp. 1314–1319, 1996.

[13] D. Flandre, A. Viviani, J.-P. Eggermont, B. Gentinne, and P. Jespers, "Improved synthesis of gain-boosted regulated-cascode CMOS stages using symbolic analysis and gm/ID methodology," *IEEE J. Solid-State Circuits*, vol. 32, no. 7, pp. 1006–1012, 1997.

[14] E. Alvarez and A. Abusleme, "Noise power normalisation: Extension of g_m/I_D technique for noise analysis," *Electron. Lett.*, vol. 48, no. 8, pp. 430–432, 2012.

[15] L. Fabris and P. Manfredi, "Optimization of front-end design in imaging and spectrometry applications with room temperature semiconductor detectors," *IEEE Trans. Nucl. Sci.*, vol. 49, no. 4, pp. 1978–1985, Aug. 2002.

[16] W. Liu, X. Jin, X. Xi, J. Chen, M.-C. Jeng, Z. Liu, Y. Cheng, K. Chen, M. Chan, K. Hui, J. Huang, R. Tu, P. K. Ko, and C. Hu, *BSIM3v3.3 MOSFET Model, User's Manual*.   Berkeley, CA: Department of Electrical Engineering and Computer Sciences, University of California, 2005.

[17] Star-Hspice Manual2001 ed. Avant! Corporation, 2001.

[18] MOSIS [Online]. Available: http://www.mosis.com